Society of Petroleum Engineers

SPE-183789-MS

Toward an Integrated and Realistic Interpretation of Continuous 4D Seismic Data for a CO_2 EOR and Sequestration Project

Philippe Nivlet, Robert Smith, Michael A. Jervis, and Andrey Bakulin, Saudi Aramco

This paper was prepared for presentation at the SPE Middle East Oil & Gas Show and Conference held in Manama, Kingdom of Bahrain, 6-9 March 2017.

Abstract

In 2015, Saudi Aramco commenced its first carbon capture and sequestration project, with carbon dioxide (CO_2) injected into a small area of a carbonate reservoir located in the Eastern Province of Saudi Arabia. To monitor the expansion of the CO_2 plume, continuous 4D seismic data is being recorded at an average rate of one survey per month. The interpretability of data requires: (1) a high degree of repeatability, which has been achieved through dedicated acquisition and processing, (2) sufficient sensitivity of seismic data to injected CO_2, (3) accurate characterization of reservoir heterogeneity, and (4) a fit-for-purpose workflow to interpret time-lapse seismic images. This paper focuses on the last three points.

First, a rock physics model (RPM) is calibrated from available well data (well logs, fluid analysis), showing that CO_2 injection causes a drop in both acoustic impedance and Poisson's ratio of 6% at the well log scale, leading to moderate seismic data sensitivity, and therefore, a priori challenging interpretation. Second, the RPM allows estimating changes in elastic parameters corresponding the CO_2 saturation variations predicted at different calendar times by the history matched reservoir model. Synthetic seismic data is modeled, to which we add realistic seismic noise, directly derived from seismic monitoring data. A multivariate statistical model between 4D amplitude maps and CO_2 concentration is calibrated. Finally, this model is used to produce maps of CO_2 concentration as predicted by the seismic data. Uncertainty is propagated throughout this approach, which allows us to use statistical methods to highlight regions where a 4D signal is strong enough to produce a detectable response.

Besides providing an integrated interpretation of 4D seismic, the proposed approach also quantifies the impact of seismic data uncertainty, providing a more realistic, and therefore, more useful interpretation.

Introduction

Time-lapse, or 4D seismic data, has received a lot of attention from the oil industry since the late 1980s. Numerous case histories have been published in the literature where 4D seismic has detected bypassed hydrocarbons and pressure compartmentalization, leading to successful production optimization (see Fanchi et al. (1999) for an exhaustive review of the early projects). This technique consists of acquiring multiple 3D seismic volumes at different calendar times during production and injection activities. Changes in pressure and fluid saturation, caused by reservoir production (or fluid injection) can result in changes in elastic

properties, which in turn induce variations in the seismic signal. The magnitude of these changes on seismic traces depends on many parameters, including the nature of the rocks and fluids in and around the reservoir, and the amplitude of reservoir parameter changes. This effect will be detectable in the case where the 4D signal is higher than the local noise affecting seismic data.

In this paper, we present a case study based on an onshore 4D seismic project to monitor carbon dioxide (CO_2) injection in the Eastern Province of Saudi Arabia. Seismic monitoring is *a priori* a major geophysical challenge in such a harsh environment. First, the highly complex and changing near surface inhibits both imaging and data repeatability. Strong noise generated by karsts and thick sand dunes obscure reflection events, while dune migration and seasonal variations lead to high non-repeatability between surveys. Compounding the problem further, low levels of 4D signal are predicted due to the injection of CO_2 in a stiff carbonate reservoir. After having acquired seismic data continuously over 12 months, the 4D signal still remains small and difficult to interpret. Subsequently, we show in this paper that we can take advantage of these first early surveys to properly model the seismic data uncertainty, and therefore, predict when the expected changes predicted by the current reservoir model will start being detectable.

Seismic Monitoring Project

To maximize the chances of monitoring success, a highly repeatable acquisition system has been deployed to enable the observation of small reservoir changes. A hybrid system consisting of buried receivers and surface vibroseis sources was selected, Fig. 1, due to significant improvements in data repeatability and imaging compared to conventional surface acquisition (Bakulin et al., 2012). The system comprises over 1,000 sensors at a depth of 50 m to 80 m and more than 100,000 shot points on a dense 10 × 10 m grid.

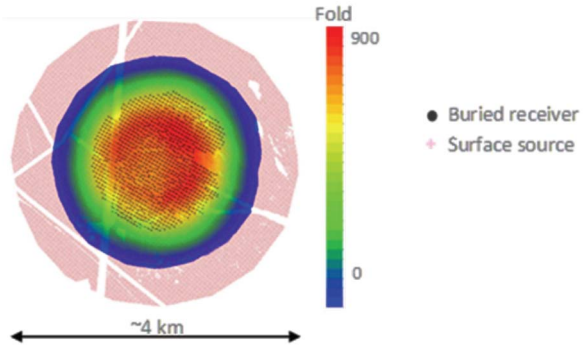

Figure 1—Geometry of the hybrid acquisition system used for CO_2 monitoring. A total of 1003 four-component sensors have been buried 50 m to 80 m below the surface on a 50 × 50 m grid. A dense vibroseis source grid (10 × 10 m) ensures high fold data to improve signal-to-noise ratio (SNR).

Monthly surveys have been acquired since mid-2015, and the system has achieved excellent repeatability between surveys so far. The normalized root mean square (NRMS) is a common measure of data repeatability that is sensitive to amplitude, time and phase changes between surveys (Eq. 1, Kragh and Christie, 2001). NRMS is defined as:

$$NRMS_j(x) = 2 * \frac{RMS\left(A_j(x) - A_0(x)\right)}{RMS\left(A_j(x)\right) + RMS\left(A_0(x)\right)} \quad (1)$$

where $NRMS_j(x)$ represents the NRMS computed over a given time window at the position x for the *jth* monitor survey, $A_j(x)$ and $A_0(x)$ are, respectively, the parts of seismic traces from the *jth* monitor and from the baseline survey at position x, and RMS is the RMS of the trace amplitudes computed over this interval.

NRMS values can range from 0%, indicating perfectly repeatable traces, to 200% for traces of opposite polarity. Between closely spaced surveys, mean NRMS values of less than 5% for the reservoir of interest

have been achieved (Bakulin et al., 2016). Consequently, a significant increase in 4D noise has been observed during the rainy season (November to April), with changes in near surface properties appearing to result in small waveform changes. Figure 2 shows the average NRMS based on pre-stack early arrival analysis, which clearly shows a cyclical trend in data repeatability. Significant processing effort has been able to greatly reduce these effects, but an imprint remains that may inhibit the detection of CO_2 related signal.

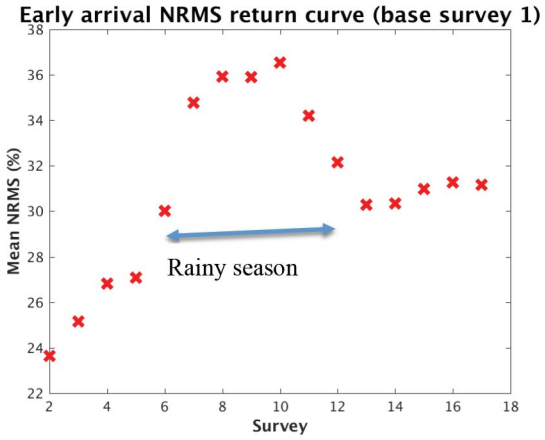

Figure 2—Mean NRMS of early arrivals compared to survey number one. A large increase in 4D noise is evident with the onset of the rainy season during survey 6. Survey 12 signals the onset of summer.

Integration of Seismic Data

Rock Physics Model

Simulation-to-seismic is a process used to predict the elastic properties of a reservoir (Vp, Vs and density) from geological and reservoir simulation information. Key to this method is the rock physics model (RPM), which links the elastic parameters to porosity, saturation and pressure inputs. In this study, a RPM was calibrated from nine well logs available in the area. Vp, Vs and density profiles were used to calculate the saturated elastic parameters (bulk and shear modulus) at each measurement point, then the fluid effect predicted (using the saturation log) and removed to estimate the dry frame bulk modulus. The best-fit relationships between the dry rock elastic parameters (bulk/shear modulus and density) and total porosity were then derived, which serve as the RPM for this study.

Next, the changes in the elastic rock properties due to changing fluid mixes are predicted using the RPM and Gassmann fluid substitution (Gassmann, 1951). Porosity, saturation and pressure inputs were taken from a history matched reservoir simulation model based on the first 12 months of injection. The dry frame elastic parameters at each cell are first derived as a function of porosity using the previously defined relationships. The effective fluid properties are then estimated at each time step of the simulation model. Individual fluid properties for oil and brine are predicted using the FLAG14 calculator based on the empirical work of Han and Batzle (2000), while the acoustic properties of supercritical CO_2 were based on equation of state models (Kunz and Wagner, 2012). The effective bulk modulus of the fluid mix is calculated using the Woods method, which assumes homogenous mixing of the fluids in the pore space. The effective density is simply the arithmetic mean of the fluids weighted by saturation.

The primary effect of CO_2 is to reduce the effective bulk modulus of the fluid when replacing more incompressible oil or brine. A small reduction in density is also expected. The subsequent changes in elastic properties of the saturated rock following Gassmann fluid substitution are shown in Fig. 3 after 12 months of injection. Here we observe maximum reductions in Vp and density of approximately 5% and

2%, respectively. The minor increase in Vs is due to the small reduction in bulk density resulting from CO_2 injection.

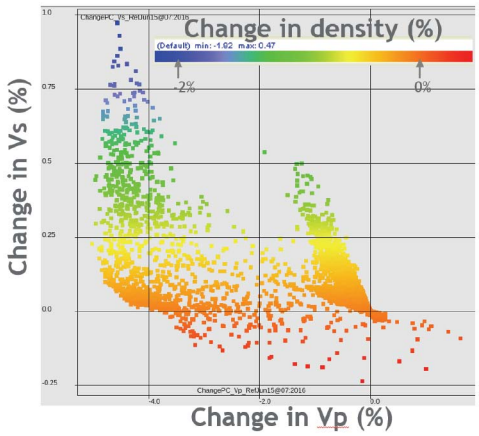

Figure 3—Cross-plot showing modeled changes in saturated rock elastic parameters after 12 months of CO_2 injection. The largest changes occur due to CO_2 replacing oil/brine, which results in a smaller Vp and density. A small increase in Vp occurs where water replaces oil.

Seismic Data Interpretation

Seismic data has low resolution with respect to the target of interest. Therefore, we can only produce a map of average properties from seismic amplitudes. The well's log data analysis shows that two parameters control acoustic impedance (AI) and therefore full-stack seismic amplitudes: porosity and lithology, Fig. 4.

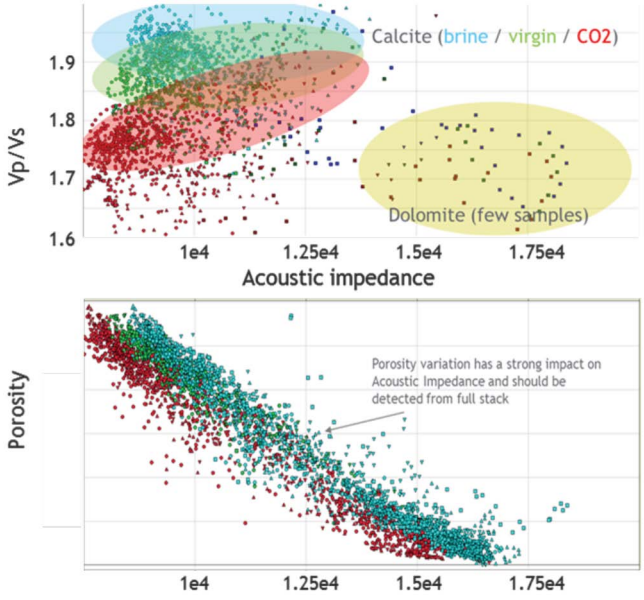

Figure 4—*Cross-plots of AI vs. Vp/Vs (up) and AI vs. porosity in the reservoir showing the impact of porosity, fluid and lithology on elastic parameters.*

On one hand, variability in average porosity does not seem to vary significantly from well to well, and a seismic prediction of porosity may therefore be of little interest. On the other hand, lithology in the reservoir is made of two components: calcite and dolomite. Variability in dolomite proportion varies from 0% to 30% of the total reservoir thickness. Based on this observation, two classes have been defined depending on its dolomite content (with a threshold at 20%). We have calibrated a statistical classification model (quadratic discriminant analysis) based on the vertical succession of seismic trace amplitudes in the reservoir window

(Fournier and Derain, 1995). Training samples are made of all the traces within 100 m of each well. Cross-validation scores exceed 85%. Figure 5 displays the map of probability of dolomite stringers resulting from the analysis. Toward the edge of the survey, the higher probabilities are likely caused by lower fold, therefore lower SNR ratio data, and so should not be trusted. Elsewhere, the prediction is in line with the lithology interpreted at the well locations. This map can be used as a local average to the 3D lithology model and used as an input to production and injection data history matching.

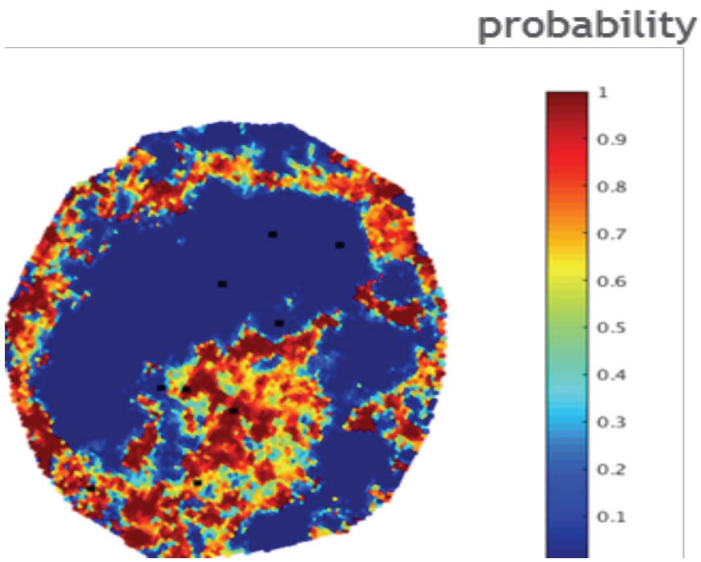

Figure 5—A probability map displaying the variability of dolomite stringers. Zones in blue are predicted to have low dolomite content.

Seismic Data Modeling

A history matched geomodel provides a dynamic model of predicted CO_2 concentrations at different calendar times. For this particular paper, we consider five calendar times, corresponding respectively to the start of CO_2 injection (baseline survey), and 6, 12, 18 and 24 months after this date. Corresponding seismic amplitude volumes will be named respectively A_0, A_6, A_{12}, A_{18} and A_{24}. Different volumes to the baseline A_0 will be referred to as D_6, D_{12}, D_{18} and D_{24}, respectively. Figure 6 displays the cumulated CO_2 column height predicted from 6 to 24 months after the start of injection.

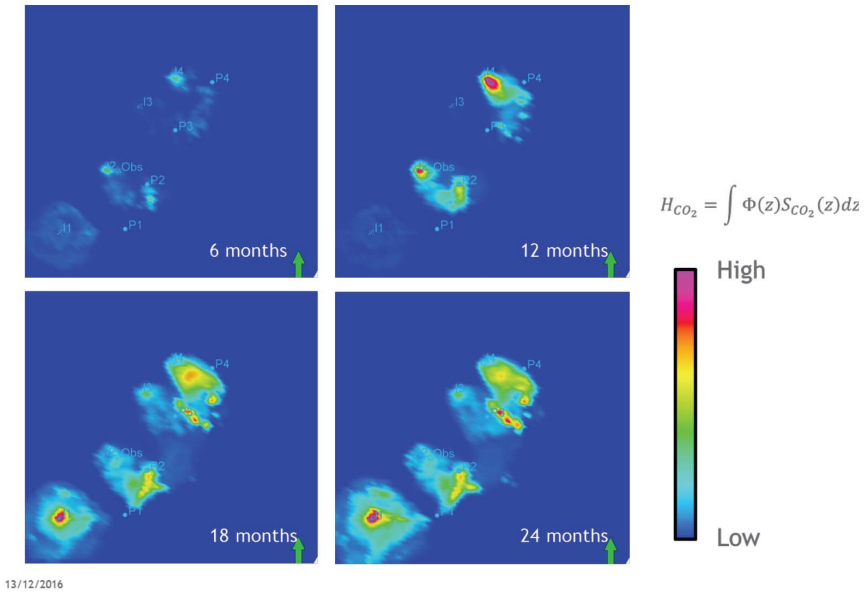

Figure 6—Predicted CO_2 column height estimated from the history matched model.

The RPM described previously allows transforming these CO_2 concentrations to elastic parameters at each calendar time. In turn, these elastic parameter cubes are converted to reflectivities based on the Zoeppritz equation. By convolving the latter with the wavelet extracted from the actual seismic data, we obtain synthetic seismic amplitude cubes that can be used for quantitative analysis. We consider at each position of the survey a 40-ms long analysis window, centered on the interpreted mid-reservoir seismic marker. This window corresponds roughly to the full reservoir window and amplitudes are extracted every 2 ms from the four available 4D amplitude difference volumes.

Figure 7 shows a vertical section through seismic amplitudes from the baseline survey flattened on the reservoir reflection (top). Time-lapse amplitude differences are small in general, as can be seen in the lower picture where differences have been amplified 10 times. Figure 8 displays the four NRMS maps calculated for each of the four 4D surveys over the reservoir window. Qualitatively, NRMS values are highly correlated to the CO_2 column height: the higher the CO_2 column, the higher the NRMS. Quantitatively, the correlation between the two quantities is 0.6. On average, the expected 4D signal is small: less than 5% for D_6, and peaking at around 10% for the later surveys.

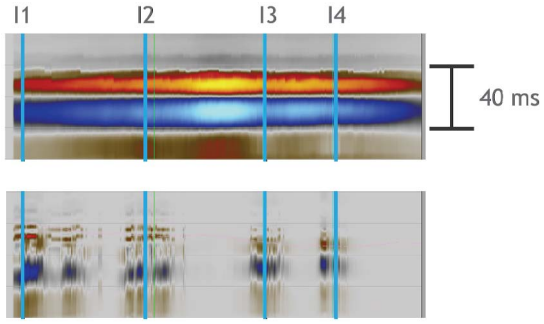

Figure 7—Seismic section across the four injector wells for the baseline (top) and 4D difference (magnified 10 times) predicted after 24 months of injection.

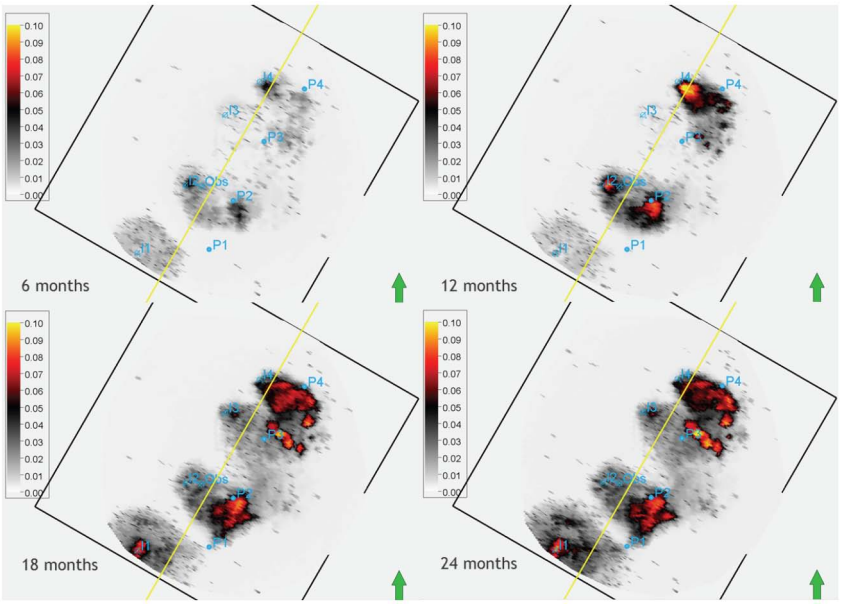

Figure 8—NRMS maps (%) corresponding to D6, D12, D16 and D24.

Sensitivity Study

Methodology

Statistical Modeling of CO_2 Height. The following statistical analysis is completed simultaneously over all the traces of the different data vintages/surveys. Subsequently, the analyzed dataset has 21 variables — seismic amplitudes in the reservoir window. To reduce the redundancy between the different variables, we first apply Principal Component Analysis to the dataset. We keep the first four components, which account for 96% of the total variance. In the following, the function from amplitudes to principal components is referred to as *f*.

A linear regression model is then calibrated between the cumulative CO_2 height and these four principal components. The resulting correlation coefficient R^2 is 0.6, showing that the CO_2 height has an effect on seismic amplitude, although the model has significant uncertainty. The latter can be captured from the crossplot between modeled and real CO_2 heights, Fig. 9. The cloud of points shows some scattering along the first bisector line, indicating that the linear model is not biased. Furthermore, the prediction error is approximately independent of the predicted variable,

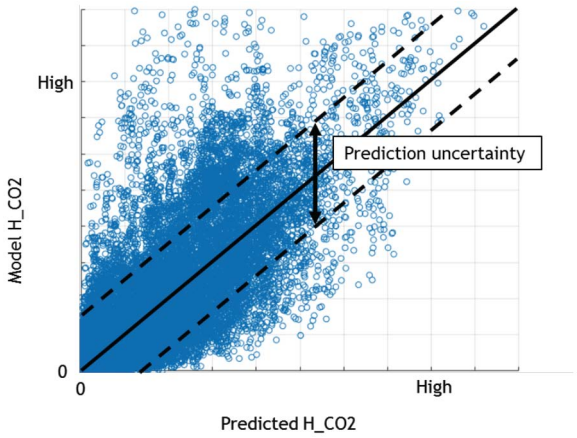

Figure 9—CO_2 height predicted by the linear model from seismic attribute maps vs. real CO_2 height.

4D Noise Modeling. The first monitor survey was recorded only one month after the start of the CO_2 injection. Therefore, the amplitude differences between this survey and the baseline can be considered as a realization of the random variations of the 4D seismic noise. A 3D variogram is estimated from this difference cube using a 200-ms time window centered on the reservoir. Vertically, the variogram is modeled by a cosine-exponential model, while horizontally it is the sum of two nearly isotropic spherical models, Fig. 10.

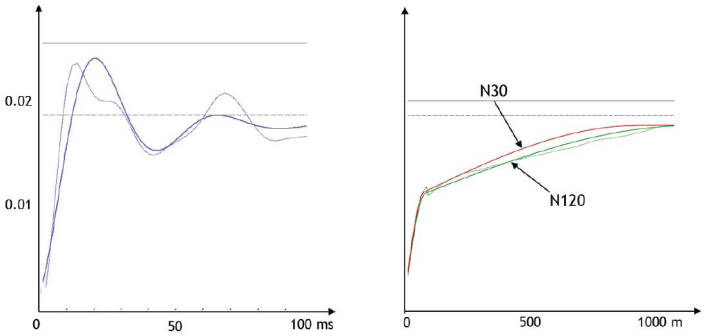

Figure 10—4D noise vertical (left) and horizontal (right) variograms. Thin lines are measured and bold lines are modeled variograms.

Two additional elements influence the noise model. First, the average 4D noise varies with calendar time, previously seen in Fig. 2. To account for the noise level increase during the rainy season, we add an extra 30% to the variance of these variograms for surveys A_6 and A_{18}, which corresponds to observations. Second, noise has been increased on the edges of the survey to account for the lower seismic fold in this area in comparison with the center.

Sequential Gaussian simulation is used to generate 400 independent realizations of the noise. Figure 11 displays a section and an RMS map extracted from the reservoir window from one of these simulations.

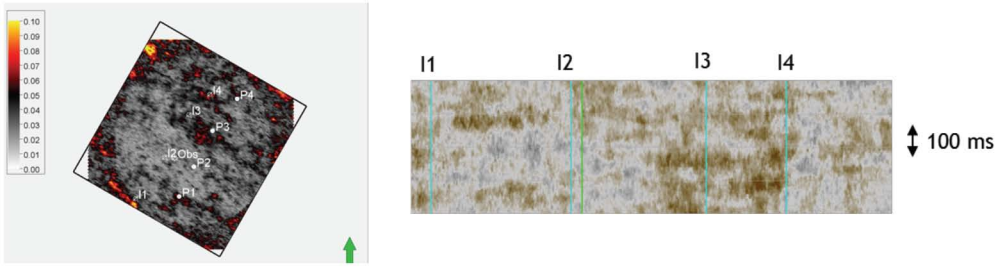

Figure 11—Vertical RMS average (left) and vertical random line through the four injectors for realization #2 of the 4D noise.

These noise realizations are then added to the synthetic 4D cubes for each of the four studied monitor surveys to obtain realistic 4D signal realizations.

Results and Discussion

To obtain the final realization of CO_2 height, we consider successively each of the realizations of the 4D signal. Then, we extract the same 21 amplitude maps in the reservoir window as in the noise-free synthetic dataset. Next, these amplitude maps are transformed to principal component maps using the transformation f, and the regression model is used to transform them to the CO_2 height. The result is finally perturbed by adding random noise with no spatial correlation and a standard deviation of 0.7 to account for the modeling errors.

For each survey, and at each position, we create 100 realizations of the predicted CO_2 height. We test whether this predicted CO_2 height is statistically significant or not with a Student's test. The significance

level for the test is set to 5%. Figure 12 displays the results of this analysis for each of the four calendar dates. Areas in red correspond to places where seismic is expected to give a significant response.

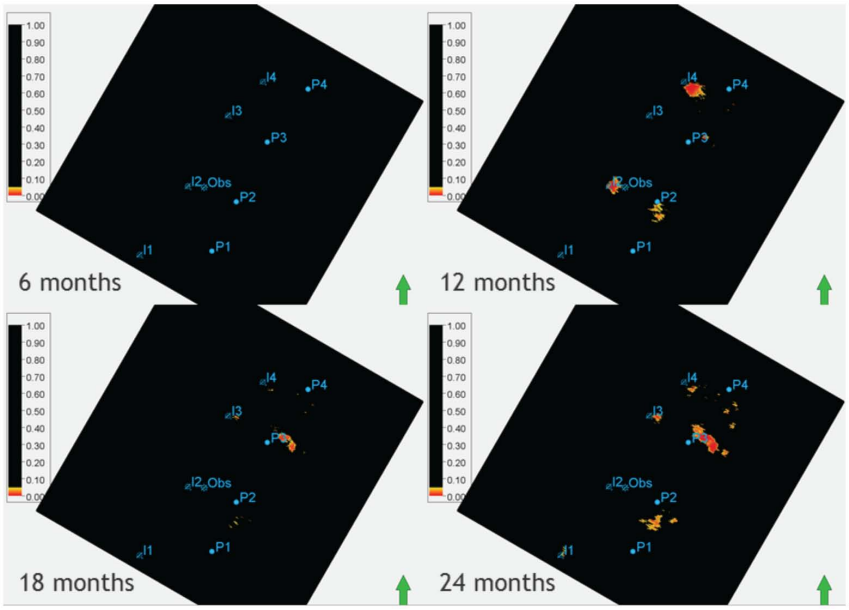

Figure 12—Maps of CO_2 detectability from seismic.

At T_0 + 6 months, seismic is insensitive to the injected CO_2, which has been verified by the acquired data. The detectability level is reached very locally around injector I_4 after 12 months. Other areas above the detectability level are probably too small to be interpretable from real seismic data. The detectability drops again after 18 months due to the increased noise observed during the rainy season. Finally, detectability increases at T_0 + 24 months. Significant anomalies are detected close to producers P_2 to P_3 where the CO_2 height predicted by the reservoir model is high. Note that in the last survey, the seismic signal hardly reaches the detectability level close to injector I_1, despite the large quantity of CO_2 injected into this well. This is due to the lower SNR ratio of seismic in this area because of the lower fold on the margins of the survey area.

Conclusions

We have presented a methodology to evaluate the sensitivity of seismic data to reservoir changes due to CO_2 injection in a stiff carbonate reservoir. The success of such an approach relies on integrating, in a consistent manner, outputs from different displines such as rock physics, geomodeling, reservoir engineering, geostatistics and seismic interpretation. The study showed that the two main elements influencing the seismic detectability are the total quantity of CO_2 accumulated locally and the noise level. Results have been validated with field data that had already been acquired at the date of the study and can be used as a feasibility study for surveys to come.

Acknowledgments

We would like to thank Saudi Aramco for allowing us to publish this work. We would like to acknowledge Rudi Lubbe for his work on the RPM.

References

Bakulin, A., Burnstad, R., and Jervis, M. 2012. Evaluating Permanent Seismic Monitoring with Shallow Buried Sensors in a Desert Environment. SEG 82nd Annual Meeting, Las Vegas, Nevada, pp. 1–5.

Bakulin, A., Smith, R., and Jervis, M. 2016. Processing and Repeatability of 4D Buried Receiver Data in a Desert Environment. SEG 86th Annual Meeting, Dallas, Texas, pp. 5405–5409.

Fanchi, J. R., Pagano, T. A. and Davis, T. L. 1999. State of the Art of 4D Seismic Monitoring: The Technique, the Record, and the Future. *Oil and Gas Journal*, **97** (22).

Fournier, F. and Derain, J.-F. 1995. A statistical methodology for deriving reservoir properties from seismic data Geophysics, **60** (5): pp. 1437–1450.

Gassmann, F. 1951. Elastic Waves through a Packing of Spheres: Geophysics, **16**: 673-685.

Han, D.-H. and Batzle, M. 2000. Velocity, Density and Modulus of Hydrocarbon Fluids – Data Measurement. SEG 70th Annual Meeting, Calgary, Alberta, Canada, pp. 1862–1876.

Kragh, E. and Christie, P. 2001. Seismic Repeatability, Normalized RMS and Predictability. SEG 71st Annual Meeting, San Antonio, Texas, pp. 1656–1659.

Kunz, O. and Wagner, W. 2012. The GERG-2008 Wide-Range Equation of State for Natural Gases and Other Mixtures: An Expansion of GERG-2004. *Journal of Chemical & Engineering Data*, **57** (11): pp. 3032–3091.